

K-SHELL PHOTOIONIZATION AND PHOTOABSORPTION OF Ne, Mg, Si, S, Ar, AND Ca

M. C. WITTHOEF¹, M. A. BAUTISTA², C. MENDOZA³, T. R. KALLMAN¹, P. PALMERI⁴, AND P. QUINET⁴

¹ NASA Goddard Space Flight Center, Code 662, Greenbelt, MD 20771, USA

² Department of Physics, Virginia Polytechnic and State University, Blacksburg, VA 24061, USA; bautista@vt.edu

³ Centro de Física, Instituto Venezolano de Investigaciones Científicas (IVIC), Caracas 1020A, Venezuela

⁴ Astrophysique et Spectroscopie, Université de Mons-Hainaut, B-7000 Mons, Belgium

Received 2009 February 9; accepted 2009 March 12; published 2009 April 15

ABSTRACT

We present extensive computations of photoabsorption and photoionization cross sections across the K-edge of Ne, Mg, Si, S, Ar, and Ca ions with less than 11 electrons. The calculations are performed using the Breit–Pauli R -matrix method and include the effects of radiative and Auger damping by means of an optical potential. The wave functions are constructed from single-electron orbital bases obtained using a Thomas–Fermi–Dirac statistical model potential. Configuration interaction is considered among all fine-structure levels within the $n = 2$ complex. The damping processes affect the resonances converging to the K thresholds causing them to display symmetric profiles of constant width that smear the otherwise sharp edge at the photoionization thresholds.

Key words: atomic data – atomic processes – methods: numerical – X-rays: general

Online-only material: tar files

1. INTRODUCTION

The unprecedented spectral capabilities and sensitivity of recent, orbiting X-ray telescopes (*Chandra*, *XMM-Newton*, *Suzaku*) have opened the door for quantitatively accurate studies of atomic inner-shell processes in astrophysical plasmas. This trend will continue to grow with the launch of future instruments such as the *International X-ray Observatory (IXO)*. Such inner-shell processes, particularly K-shell processes, are observed in the spectral band of the observatories from all ionic stages of the most abundant elements between oxygen and nickel (see Paerels & Kahn 2003 for a review on the subject). These spectra are extremely valuable for they can be used to diagnose the conditions of the plasma and its chemical composition. However, the diagnostic power depends on our understanding of the microphysics of the atomic systems and ultimately relies on the accuracy of the atomic data.

For the last few years, our team has dedicated significant efforts toward the study of K-shell processes and atomic data starting with the Fe ions. Complete data sets of level energies, wavelengths, Einstein A -coefficients and Auger rates for K lines in Fe II–Fe XXV have been provided by Bautista et al. (2003), Palmeri et al. (2003a, 2003b), and Mendoza et al. (2004). In order to model non-LTE spectra we also calculated data needed in representing population mechanisms, namely, photoabsorption, photoionization, and electron-impact excitation cross sections. In this respect, we found that the K-threshold resonance behavior in these continuum processes in both lowly and highly ionized species is different from that displayed by the outer-electron resonance series. For instance, Gorczyca (2000), Gorczyca & McLaughlin (2000), and Palmeri et al. (2002) showed that the K-resonance widths are dominated by radiative and spectator Auger decays that result in a Rydberg resonance series whose widths are independent of the principal quantum number and thus lead to a smearing of the K-edge. Moreover, Palmeri et al. (2002) shows the possibility of devising diagnostics based on K-edge broadening which would necessarily rely on accurate high-energy photoabsorption cross sections. On the other hand, most previous close-coupling calculations of high-energy continuum processes in Fe ions (Berrington et al. 1997; Donnelly

et al. 2000; Berrington & Ballance 2001; Ballance et al. 2001) have completely ignored spectator Auger decay, the main contributor of the K-resonance width. This deficiency has been corrected in the photoabsorption, photoionization, and electron-impact excitation calculations of Bautista et al. (2004) for Fe XVII–Fe XXIV. Photoionization cross sections for lower ionization stages of Fe were presented by Kallman et al. (2004) together with a detailed study of the formation of the K-shell spectrum in photoionized plasmas.

After the work on iron, a similar study of the K-shell spectrum of oxygen was presented in García et al. (2005). We have now turned our attention toward other astronomically abundant elements, namely, Ne, Mg, Si, S, Ar, and Ca. For these ions, calculations of energy levels, Einstein A -coefficients, and Auger rates were recently reported by Palmeri et al. (2008). In this work, we present total photoabsorption and photoionization cross sections for those ions with less than 11 electrons. For the case of photoionization, we also calculate partial cross sections where the daughter ion is left in a photoexcited K-vacancy state. All calculations have been carried out with the relativistic Breit–Pauli R -matrix (BPRM) method. Tables of the total and partial cross sections accompany this article as online tables. Full data sets are also available through the XSTAR atomic database (Bautista & Kallman 2001).⁵

2. NUMERICAL METHODS

The numerical approach used for these calculations is the same as our previous K-shell calculations and is described in Bautista et al. (2003). The wave functions and Auger widths for the present calculations are obtained using AUTOSTRUCTURE (Badnell 1986, 1997) following the results of Palmeri et al. (2008). The scattering calculations were carried out with the BPRM framework. The R -matrix method is based on the close-coupling approximation of Burke & Seaton (1971), which is solved numerically following Burke et al. (1971) and Berrington et al. (1974, 1978, 1987). One-body Breit–Pauli relativistic corrections have been introduced into the R -matrix suite by Scott

⁵ <http://heasarc.nasa.gov/lheasoft/xstar/xstar.html>

& Burke (1980) and Scott & Taylor (1982). Since interchannel coupling is equivalent to configuration interaction (CI) in the atomic structure context, the BPRM method provides a formal and unified approach to study the decay properties of both bound states and resonances.

As in the previous calculations of iron and oxygen ions, the effect of radiative and spectator Auger decay on resonances is included within the BPRM framework by means of the optical potential of Gorczyca & Badnell (1996, 2000). Here, the resonance energy with respect to the threshold energy acquires an imaginary component which is the sum of the radiative and Auger widths of the core. The radiative widths are computed from the same BPRM calculations following Robicheaux et al. (1995). The Auger widths are provided from the AUTOSTRUCTURE calculations of Palmeri et al. (2008). These effects are referred to as radiative and Auger damping since they cause resonances in the photoionization cross section to become smaller in area. The damping also makes it necessary to calculate both the photoabsorption and photoionization cross sections since not every absorbed photon will result in a photoelectron.

We use the *R*-matrix computer package of Berrington et al. (1995) for the inner region calculation and the asymptotic region code STGBF0DAMP (Gorczyca & Badnell 1996; N. R. Badnell, unpublished) is used to compute the photoabsorption and photoionization cross sections where the effects of both radiation and Auger dampings are included. The contributions to the cross sections from the long-range potentials in the outer region solutions are included for all ions.

Due to the number of ions covered in the present work, we have developed a script to perform the calculations more efficiently. As part of the script, an automatic mesh refinement scheme is used to resolve all of the important K-shell resonances. This scheme consists of a tree method to update the energy mesh spacing in regions where the integrated cross section area is not yet converged by successively dividing the energy range. This is followed by a scan method which adds more energy points around partially resolved resonances. The automatic mesh refinement is most important for the Li-like ions which have no KLL Auger channel and therefore no Auger broadening of the resonances. However, for all sequences, this method is important to get the correct resonant enhancement near the K-edge.

The target expansion for each ion includes all $1s^2 2l^n$ and $1s 2l^{n+1}$ configurations where $2+n$ is the number of electrons in the photoionized (target) ion. We include enough continuum basis orbitals so that they span from threshold to at least four times the energy of the K-edge. This choice gives reliable cross sections up to at least twice the energy of the K-edge. Cross sections are calculated from all levels in the ground configuration of the parent ion. For neutral Ne, we use a larger target expansion containing the $1s^2 2s^2 2p^5$, $1s^2 2s 2p^6$, $1s^2 2s^2 2p^4 nl$ ($nl = 3s, 3p, 3d, 4s, 4p$), $1s^2 2s^2 2p^3 3s^2/3p^2$, $1s^2 2s 2p^5 3s/3p$, $1s 2s^2 2p^6$, $1s 2s^2 2p^5 3s/3p$, and $1s 2s 2p^6 3s/3p$ configurations. Due to the size of this target, the neutral Ne calculations were restricted to *LS* coupling.

We find oscillations in some cross sections calculated using the length gauge at high scaled energies (z^2 Ry, where z is the difference between the nuclear charge and the number of electrons in the target species). For these cases, it is important to switch to using the velocity gauge to obtain a smooth high-energy cross section. Therefore, in the present calculations, the cross section above the K-edge was determined using the velocity gauge for all ions. While discontinuities can occur in the cross section when switching gauges, the size of such steps in the present

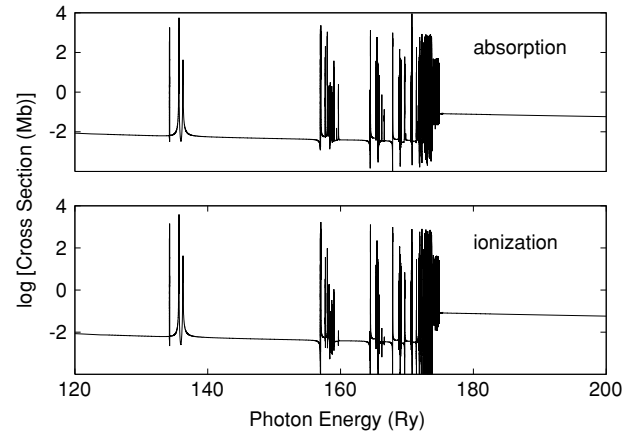


Figure 1. Photoabsorption (top panel) and photoionization (bottom panel) cross sections of Li-like Si.

work is small (less than 10%). For many ions ($z \lesssim 6$), we use the velocity gauge at all energies due to oscillations seen within and below the resonance region when using the length gauge.

We use *R*-matrix to calculate cross sections up to about twice the energy of the K-edge. However, for modeling purposes, it is useful to have the total and partial cross sections available to higher energies. Therefore, we extend our cross sections up to 1000 Ry with more approximate methods. Beyond the K-edge, the total photoionization and photoabsorption cross sections are equivalent and we use AUTOSTRUCTURE (Badnell 1986, 1997) to provide the cross section beyond the highest *R*-matrix photon energy. The high-energy cross section from AUTOSTRUCTURE is scaled so that it matches smoothly with the *R*-matrix cross section at the highest *R*-matrix energy. To extend the partial photoionization cross sections, we employ two methods. For the partials allowed by the photoionization selection rules, AUTOSTRUCTURE is used in the same manner as with the total cross sections. For channels which are only nonzero through mixing, we use a simple power-law extrapolation of the *R*-matrix results. While this latter method is prone to large errors at 1000 Ry, we extrapolate these weak partials so that they scale with energy in roughly the same way as the strong partials.

3. RESULTS

As in previous studies of inner-shell photoionization of iron, we find that cross sections near the K-threshold are dominated by a series of symmetric resonances of constant width which cause smearing of the K-edge. This is due to KLL Auger transitions where the outer electron with principal quantum number n remains as a spectator. Thus, damping of $n > 2$ resonances along the Rydberg series is practically independent of the resonance principal quantum number. The Li-like ions are an exception to this since there are too few electrons for the KLL Auger process to occur. For these ions, the resonances remain very narrow and asymmetric. In Figure 1 are shown the photoabsorption and photoionization cross sections for Li-like Si. There is little difference here, and in all the Li-like ions, between absorption and ionization due to the small amount of radiation damping. For the rest of the isoelectronic sequences, however, Auger damping broadens the absorption resonance features and radiation damping significantly damps the resonances of the ionization cross section near the K-edge. As an example, we show the Be-like Si cross sections in Figure 2. The absorption resonances now have a symmetric profile which is the reason for the smeared K-edge around 170 Ry. Were

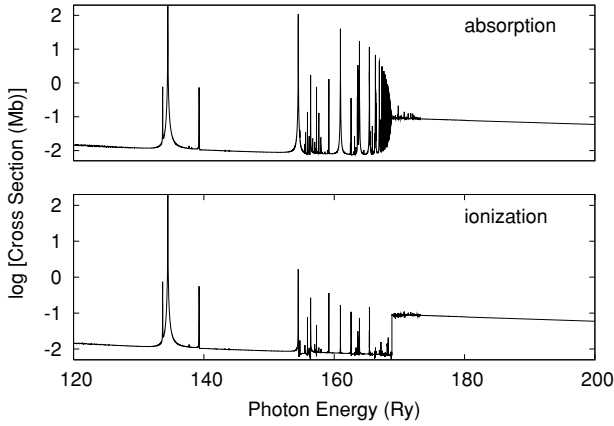


Figure 2. Photoabsorption (top panel) and photoionization (bottom panel) cross sections of Be-like Si.

the resonances asymmetric, the edge would have been much sharper as is seen in Li-like Si. The resonances in the Be-like Si photoionization cross section are increasingly damped as you approach the K-edge.

When radiation damping is taken into account, the photoabsorption and photoionization cross sections must be treated separately. This is most apparent near the K-edge where the photoionization resonances are almost completely damped. In Figure 3, we compare the photoabsorption and photoionization cross sections for C-like Ca. In the case of photoabsorption, the K-edge is completely lost due to resonant enhancement, but the edge is still well defined in the photoionization cross section. In fact, we see two edges; the first at 344.9 Ry is where the $1s\ 2s^2\ 2p^2\ ^2P_{1/2}$ channel opens up and the second at 346.6 Ry where the $^2P_{1/2}$ channel is opened. The cross sections to the other $1s\ 2s^2\ 2p^2$ levels are too small to result in edges in the photoionization cross section (due to K-shell photoionization selection rules discussed later). Also in the figure is a curve showing the photoabsorption cross section convolved with a Gaussian of width $\Delta E/E = 0.001$, which is representative of the resolution of currently orbiting X-ray telescopes. If the resonances are fully resolved, the convolved photoabsorption cross section should smoothly cross the K-edge, which is seen in the figure. This illustrates that for current (and near-future) telescopes, the instrument resolution will always smear the K-edge region much more than due to the natural width of the resonances with or without including Auger damping. Auger damping is crucial, however, for obtaining the correct photoionization cross section.

For the purpose of building spectral models we also compute partial photoionization cross sections for all ions. Thus, it is worth examining some isoelectronic trends of the background partial cross sections above the K-edge. It is known that the partial cross sections do not necessarily scale with the statistical weight of the initial state or the remaining photoionized core. Rau (1976) derives a general expression for the partial photoionization branching fractions, ζ , for valence-shell photoionization which predicts a deviation from statistical weighting and agrees well with experiment. We find, however, that his expression does not predict what is seen in our calculations of K-shell processes. This is not surprising since Rau was considering only valence-shell photoionization where there is at most one open subshell. For inner-shell processes, more than one open subshell is possible and care must be taken to conserve the total spin of the photoionized electron and the remaining electrons in its initial subshell. Following Rau's method, we rederive the branching fraction formula where we keep the coupling between the two

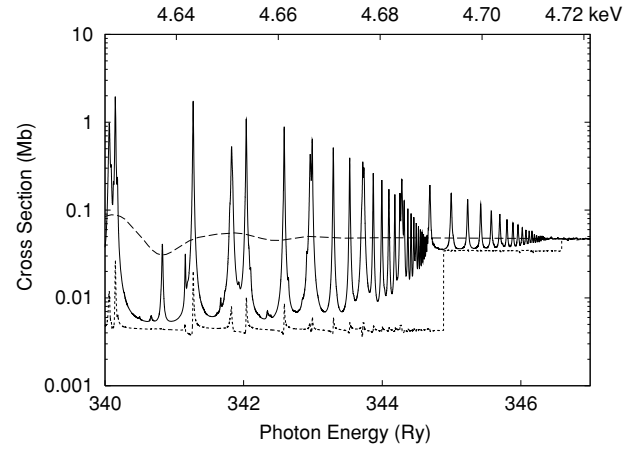


Figure 3. Photoabsorption (full curve) and photoionization (dotted curve) cross sections for C-like Ca near the K-edge. The dashed curve shows the photoabsorption cross section convolved with a Gaussian of width $\Delta E/E = 0.001$. The top axis gives the photon energies in keV.

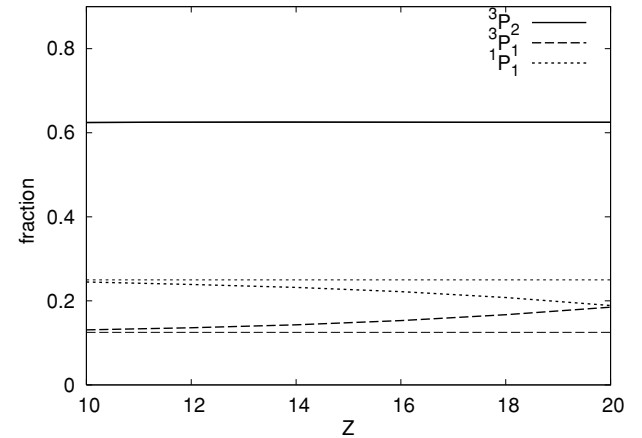


Figure 4. Fraction of partial photoionization cross section of F-like ions to the $1s\ 2s^2\ 2p^5$ levels. The bold curves are the calculated results and the faint curves are from Equation (1).

1s-electrons distinct from the remaining electrons. In this way, we can force the total spin of the remaining 1s electron and the photoionized electron to remain zero. As with Rau (1976), we assume LS -coupling for the initial state and jj -coupling between the remaining core and photoionized electron. Summing over all angular momenta of the outgoing electron, we obtain

$$\zeta = (2s_c + 1)(2j_c + 1)(2J' + 1) \left\{ \begin{matrix} S' & s_c & 1/2 \\ j_c & J' & L' \end{matrix} \right\}^2 \delta(L', l_c), \quad (1)$$

where s_c , l_c , and j_c are the spin, orbital, and total angular momenta of the photoionized core, S' , L' , and J' are angular momenta of the initial state and the quantity in curly brackets is a Wigner 6-j symbol. Implicit in the 6-j symbol is the selection rule, $j_c = J' \pm 1/2$. Apart from level mixing, this selection rule and $l_c = L'$, severely restrict which partials will have a nonzero cross section. Further summing this expression over the photoionized ion spin, s_c , we obtain

$$\sum_{s_c} \zeta = (2j_c + 1) \delta(L', l_c) \Delta(j_c, 1/2, J'), \quad (2)$$

where $\Delta(a, b, c)$ represents the triangle relations between a , b , and c and, in this case, results in the selection rule on j_c .

In Figure 4, we look at direct K-shell photoionization of the F-like system, which has a ground state of $^2P_{3/2}$, leaving the

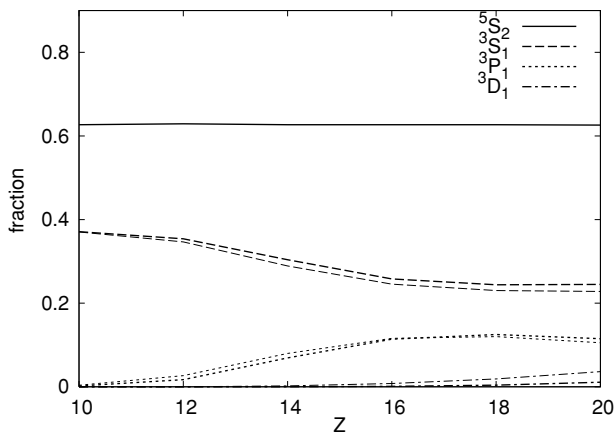


Figure 5. Fraction of the partial photoionization cross sections (bold) of N-like ions to the $1s\ 2s^2\ 2p^3$ levels. The faint curves show the mixing fractions of the 3S_1 level scaled so that the total fraction is equal to the total cross section fraction to the $J = 1$ levels.

ion in the $1s\ 2s^2\ 2p^5$ configuration (having levels $^3P_{0,1,2}$ and 1P_1). The fraction of the total cross section to the levels of this configuration is shown in the figure as a function of Z . Due to the selection rule, $j_c = J' \pm 1/2$, the cross section to the 3P_0 level is essentially zero and not shown. The bold curves are the calculated results and the faint curves show the prediction from Equation (1). At low Z , there is excellent agreement between the predicted and calculated results. As Z is increased, however, there appears to be strong mixing between the two $J = 1$ levels. In fact, these levels are only mixed at the few percent level; the deviation between the calculations and predictions is due to the breakdown of LS -coupling at higher Z . At larger nuclear charges jj -coupling between subshells (still LS -coupling within a subshell) results in a better description of the target, so we rederive Equation (1) using this coupling scheme and get an expression identical to Equation (2). Therefore, despite the break-down of LS -coupling at high Z , the partial cross sections to a given j_c are always proportional to $(2j_c + 1)$ which is what is seen in the figure.

While mixing was not important for the F-like system, it can still be important in other systems. In Figure 5, we show the fractions for the N-like system which has a ground state of $^4S_{3/2}$. In this case, there is appreciable mixing between the $J = 1$ levels. Since the initial state has $L = 0$, only the 3S_1 and 5S_2 levels should have a nonzero partial cross section, yet the fraction to the 3P_1 and 3D_1 levels increases at higher Z . The faint curves show the mixing fractions of the 3S_1 level scaled so that the sum of the mixing fractions is the same as the sum of the partial cross section fractions for $J = 1$. The agreement is very good implying that mixing is the reason for the changing fractions with Z .

4. SUMMARY AND CONCLUSIONS

Total photoabsorption and photoionization cross sections have been computed for the K-shell of all ions with electron occupancy $N < 11$ for Ne, Mg, Si, S, Ar, and Ca. Partial photoionization cross sections have also been calculated for the same ions. Radiative and spectator Auger dampings are accounted for in detail and the energy region around the K-threshold was properly delineated for each ion. All data are provided as online tables accompanying this article and can also be obtained through the XSTAR atomic database (Bautista & Kallman 2001) (see footnote 5).

We find that the K-shell branching fractions do not follow from the expression given by Rau (1976). Instead, for K-shell photoionization, the coupling between the two $1s$ electrons in the ground state must be explicit in the derivation of the branching fractions. The resulting expression agrees very well with the present calculations when there is little mixing between the levels of the photoionized ion. When the final levels mix strongly, we find the branching fractions follow the mixing fractions.

The data sets provided here together with the energy levels and radiative and Auger rates reported in Palmeri et al. (2008) will help modelers to carry out detail studies of K spectra of astrophysically abundant elements. Similar calculations for the lower ionization stages are in progress.

Support for this research was provided in part by a grant from the NASA Astrophysics Theory Program. M.C.W. is grateful to Nigel Badnell for many helpful discussions. P.P. and P.Q. are respectively Research Associate and Senior Research Associate of the Belgian F.R.S.-FNRS. Financial support from this organization is acknowledged.

REFERENCES

- Badnell, N. R. 1986, *J. Phys. B: At. Mol. Opt. Phys.*, **19**, 3827
 Badnell, N. R. 1997, *J. Phys. B: At. Mol. Opt. Phys.*, **30**, 1
 Ballance, C. P., Badnell, N. R., & Berrington, K. A. 2001, *J. Phys. B: At. Mol. Opt. Phys.*, **34**, 3287
 Bautista, M. A., & Kallman, T. R. 2001, *ApJS*, **134**, 139
 Bautista, M. A., Mendoza, C., Kallman, T. R., & Palmeri, P. 2003, *A&A*, **403**, 339
 Bautista, M. A., Mendoza, C., Kallman, T. R., & Palmeri, P. 2004, *A&A*, **418**, 1171
 Berrington, K. A., & Ballance, C. 2001, *J. Phys. B: At. Mol. Opt. Phys.*, **34**, 2697
 Berrington, K. A., Eissner, W., & Norrington, P. H. 1995, *Comput. Phys. Commun.*, **92**, 290
 Berrington, K., Quigley, L., & Zhang, H. L. 1997, *J. Phys. B: At. Mol. Opt. Phys.*, **30**, 5409
 Berrington, K. A., et al. 1974, *Comput. Phys. Commun.*, **8**, 149
 Berrington, K. A., et al. 1978, *Comput. Phys. Commun.*, **14**, 367
 Berrington, K. A., et al. 1987, *J. Phys. B: At. Mol. Opt. Phys.*, **20**, 6379
 Burke, P. G., Hibbert, A., & Robb, W. D. 1971, *J. Phys. B: At. Mol. Opt. Phys.*, **4**, 153
 Burke, P. G., & Seaton, M. J. 1971, *Methods Comput. Phys.*, **10**, 1
 Donnelly, D. W., et al. 2000, *ApJ*, **531**, 1168
 García, J., Mendoza, C., Bautista, M. A., Gorczyca, T. W., Kallman, T. R., & Palmeri, P. 2005, *ApJS*, **158**, 68
 Gorczyca, T. W. 2000, *Phys. Rev. A*, **61**, 024702
 Gorczyca, T. W., & Badnell, N. R. 1996, *J. Phys. B: At. Mol. Opt. Phys.*, **29**, L283
 Gorczyca, T. W., & Badnell, N. R. 2000, *J. Phys. B: At. Mol. Opt. Phys.*, **33**, 2511
 Gorczyca, T. W., & McLaughlin, B. M. 2000, *J. Phys. B: At. Mol. Opt. Phys.*, **33**, L859
 Kallman, T. R., Palmeri, P., Bautista, M. A., Mendoza, C., & Krolik, J. H. 2004, *ApJS*, **155**, 675
 Mendoza, C., Kallman, T. R., Bautista, M. A., & Palmeri, P. 2004, *A&A*, **414**, 377
 Paerels, F. B. S., & Kahn, S. M. 2003, *ARA&A*, **41**, 291
 Palmeri, P., Mendoza, C., Kallman, T. R., & Bautista, M. A. 2002, *ApJ*, **577**, L119
 Palmeri, P., Mendoza, C., Kallman, T. R., & Bautista, M. A. 2003a, *A&A*, **403**, 1175
 Palmeri, P., Quinet, P., Mendoza, C., Bautista, M. A., García, J., & Kallman, T. R. 2008, *ApJS*, **177**, 408
 Palmeri, P., et al. 2003b, *A&A*, **410**, 359
 Rau, A. R. P. 1976, in *Electron and Photon Interactions with Atoms*, ed. H. Kleinpoppen & M. R. C. McDowell (New York: Plenum), 141
 Robicieux, F., et al. 1995, *Phys. Rev. A*, **52**, 1319
 Scott, N. S., & Burke, P. G. 1980, *J. Phys. B: At. Mol. Opt. Phys.*, **13**, 4299
 Scott, N. S., & Taylor, K. T. 1982, *Comput. Phys. Commun.*, **25**, 347